Noise from a Model-Scale Vertical-Axis Wind Turbine

W. R. Graham* and C. E. Pearson†
University of Cambridge, Cambridge, UK

Vertical-axis wind turbines are an attractive option for small-scale wind-power installations. In this application, noise is crucially important. To investigate the problem, measurements taken from a model-scale turbine in a wind tunnel are considered. The sound radiated by the model is clearly evident in the cross-spectra from a pair of flush-mounted microphones. Parameter studies show that, in the normal operating range, speed is the dominant factor. The main source appears to be blade self-noise, although there are also indications of blade-wake interaction in the downstream half of the rotation path. Boundary-layer trips have a significant impact, showing that laminar instability is an important contributor to the self-noise. It will remain a risk at full scale, and its absence should be ensured at the design stage. To minimize the remaining sound radiation (at a given wind speed), configurations with lower tip-speed ratio at maximum power output should be preferred to ones having higher values of this parameter.

I. Introduction

LARGE-SCALE power generation from wind is dominated by turbines whose blades rotate about an axis parallel to the oncoming flow. However, devices which rotate about a vertical axis are also possible, and have some advantages: they are insensitive to wind direction, and their generators can be located at ground level. These features make them strong candidates for small-scale wind power. In this application, they would typically be in close proximity to local populations. Noise pollution is therefore a primary concern.

Systematic research on vertical-axis wind turbines (VAWTs) dates from the 1970s [1]. The focus was on technological viability, and noise was not considered. A key conclusion from this early work was that lift-based ('Darrieus') VAWTs are superior to drag-based ('Savonius') ones. As a result, there is now an established body of literature on the aerodynamics of Darrieus machines.

In contrast, studies of noise have only started to appear recently. The majority have been computational, with predictions made on the basis of the Ffowcs Williams-Hawkings (FWH) equation [2]. This approach requires a preliminary flow calculation to provide the noise-source parameters, and is numerically expensive. The cost can be mitigated by employing Reynolds-averaged Navier-Stokes solvers (e.g. [3, 4]), but it is doubtful that such codes are

*Senior Lecturer, Department of Engineering, Trumpington Street, Cambridge, CB2 1PZ; Senior Member AIAA.
†Graduate Student, Department of Engineering. Current address: Coda Octopus Products Ltd., South Gyle Business Park, 38 South Gyle Crescent, Edinburgh, EH12 9EB.

capable of estimating the FWH parameters accurately [5]. Direct numerical simulation of practical VAWT flows remains out of the question, and even computations based on the large-eddy-simulation concept are restricted to part-span geometries [5]. However, full-geometry calculations over a few turbine revolutions are feasible with detached-eddy simulations [6].

Apart from the difficulty of numerical predictions, there is also the problem of validation. None of the studies cited above were able to check their results against noise measurements. At best, predictions for output torque [5] or power [6] were compared against experiment, but agreement here is no guarantee that the FWH parameters were adequately characterized. Thus experimental noise data are needed not only for their own sake, but also to validate numerical approaches.

The current authors are aware of two experimental VAWT-noise studies. The first involved in situ measurements on a full-scale installation, initially with a single microphone [7] and then with an acoustic array [8]. The other was at laboratory scale, and is reported in the second author's doctoral thesis [9]. Here a model VAWT was tested in a wind tunnel equipped with a flush-mounted microphone array. A combination of spectrum analysis and beamforming was employed to analyse the data. Key findings were that tonal noise at the blade-passage frequency and its harmonics is unimportant (cf. also [10]), and that operation at speeds below the design range is associated with significantly raised noise levels. Beamforming was shown to be useful in identifying gross differences, but subject to limitations associated with array resolution and the presence of multiple sources.

The purpose of this work is to further the discussion of the measurements specifically relevant to practical operation, i.e. stochastic noise components at speeds in the design range. Here the differences between cases are relatively small, and consistent interpretation of beamforming results becomes difficult. Therefore the paper considers microphone-pair cross-spectra only. It starts with a brief summary of VAWT aerodynamics in the context of noise (Sec. II). The experiments and data processing are then described in Sec. III. Section IV presents the results, and also discusses their interpretation at the level of the experiment. Finally, their implications for practical VAWT design and operation are considered in Sec. V.

II. VAWT Aerodynamics

A. Operating Principle

The means by which a (Darrieus-type) VAWT generates power is best understood through a velocity-triangle diagram [11]. Figure 1 shows a VAWT blade rotating with azimuthal velocity U_b in an oncoming wind of speed U_∞. The flow relative to the blade has components due to its motion and due to the wind. The latter, which differs from U_∞ due to the influence of the turbine on the flow, is denoted U.

As a result of the relative flow, the blade generates a force F_b. Ideally, in the absence of drag, F_b would be

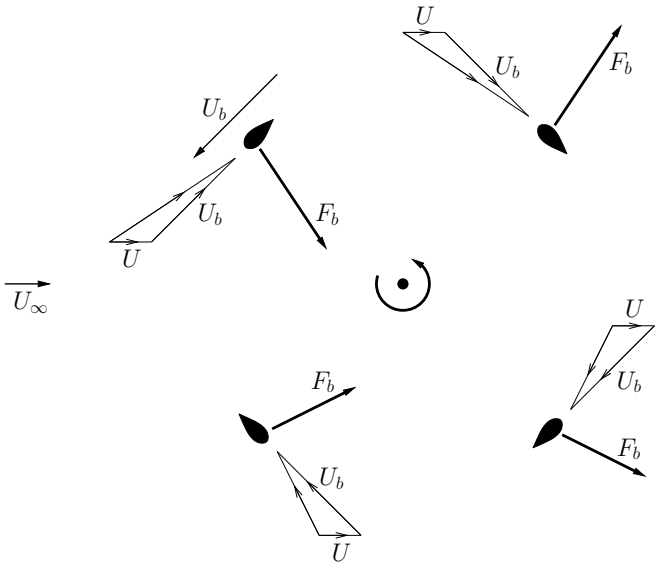

Fig. 1 Velocity triangles for a Darrieus-type VAWT blade in four azimuthal positions.

perpendicular to the relative flow. In reality, it is inclined backwards, but only to a small extent (in design-speed operation, at least). Thus F_b has an azimuthal component in the direction of rotation, and it is this component which does the work necessary to produce electrical power.

From Fig. 1 it is evident that the incidence angle of the flow relative to the blade varies with azimuthal position. A first estimate of its range follows from approximating U as U_∞, in both magnitude and direction. Then, from consideration of the furthest upstream and downstream positions, the incidence varies between $\pm \tan^{-1}(U_\infty/U_b)$.

Now recall that successful operation requires the blade force to be dominated by the lift component. This implies that stalling must be (largely) avoided, and therefore that the allowable incidence range is limited. Specifically, the tip-speed ratio (TSR) λ, defined as U_b/U_∞, must be significantly greater than 1. In practice, a Darrieus-type VAWT becomes self-sustaining between TSR 2 and TSR 3 [1].

There is also an upper limit to TSR. As it increases, the blade incidence tends towards zero, and the blade-force direction becomes less favorable. These adverse factors outweigh the increase in blade-force magnitude due to higher speed, and the power output decreases. The optimum TSR varies with turbine design; for the examples in Ref. [1] it is between 4 and 5, while the Quiet Revolution QR5 operates at TSR 3.5 [9].

B. Induction

Further insight into the VAWT blade aerodynamics can be gained by considering the impact of the turbine on the flow. As an energy-extracting device, it reduces the velocity of the oncoming air stream. Figure 2, which shows the results of a two-dimensional vortex-method calculation [12], demonstrates this effect, and allows it to be examined in more detail. Of particular interest is the difference in conditions encountered by blades traversing the upstream and

downstream arcs. The reduction in velocity is much more marked for the latter, because they lie in the wake created by the upstream traverses. Hence, while both of the nominal angle limits decrease in magnitude from $\tan^{-1}(1/\lambda)$, the downstream reduction is greater [11].

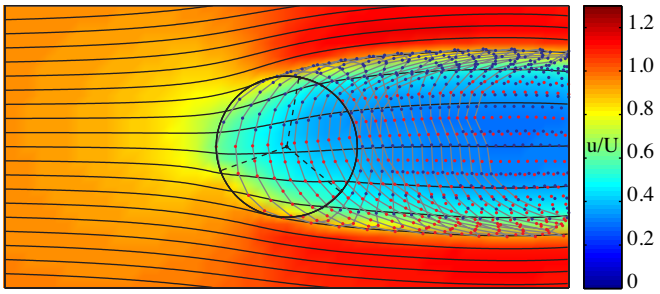

Fig. 2 Computed flow field around a VAWT ([12]; reprinted with permission). The colorbar quantity u/U is the streamwise velocity component normalized by its value at infinity.

The slowing of the oncoming flow is known as 'induction', and is characterized by the reduction as a proportion of the free-stream velocity. This quantity is known as the induction factor, and has the symbol a. It varies with both design and operational parameters; according to one theoretical model [11] it is proportional to both TSR and solidity (a measure of blade extent relative to the rotation-circle circumference). This dependence can also be deduced from an order-of-magnitude argument, as follows.

At the TSRs typical of efficient operation, the blade's effective speed and incidence at the furthest upstream position are approximately λU_∞ and $1/\lambda$ respectively. Hence the blade lift (per unit span) is proportional to $\frac{1}{2}\rho U_\infty^2 c\lambda$, where ρ is the air density and c the blade chord. The same scaling then applies to the mean streamwise force exerted by the blade on the fluid (neglecting drag contributions). The overall mean force in this direction is therefore proportional to $\rho U_\infty^2 c\lambda n_b$, where n_b is the number of blades. This force is responsible for a reduction in momentum flux of order $\rho U_\infty^2 Da$, with D the rotor diameter. Equating the two quantities yields $a \sim \lambda(n_b c/D)$, in which the bracketed term can be seen to represent the solidity.

C. Implications for Noise

For horizontal-axis wind turbines, the potential sources of sound are self-noise and interaction noise [13]. Both arise due to fluctuating pressures on the blades, differing only in the causes of such fluctuations: inherent local unsteadiness for self-noise and ambient background unsteadiness for interaction noise. The mechanisms by which local unsteadiness arises have been categorized by Brooks et al. [14], while Amiet has given a theoretical description of interaction noise [15].

For the (stochastic) noise from a VAWT, the same two components must be considered. However, the situation is more involved. At a given spanwise position, the blade section on a horizontal-axis machine is (nominally) at the same

incidence throughout the rotation arc. This means that reasonable estimates for self-noise can be made using data from steady experiments. For a VAWT, the continual change in blade flow conditions implies azimuthal variations in the associated self-noise. Even if the blade aerodynamics are taken to be quasi-steady (on the basis that the blade-flow transit time c/U_b is small compared to the rotation period), the added complexity is significant.

The blade-incidence variations will also affect interaction noise, but here a new factor enters too: in the downstream arc, the blades pass through the wake generated by their upstream transits. As the flow in this region arises from intermittent events, it will exhibit significant unsteadiness in addition to the mean induction discussed previously. This phenomenon is entirely absent for an isolated horizontal-axis turbine, and is thought not to be important even in array installations. For a VAWT, however, it must be considered, because the proximity of the wake-generating blades to the wake-encountering blades is so much greater. In what follows, it will be distinguished from contributions due to variations in the oncoming flow by referring to the latter as 'inflow-turbulence noise'.

Finally, the blades on a VAWT are not the only possible sources of aerodynamic noise. Many designs use radial spokes to link the blades to the shaft. The outer parts of these connectors travel at speeds approaching that of the blades, and are thus likewise potential sound generators.

III. Experimental Methods

A. VAWT Model

The model was made from commercially available NHP 'Razor Pro' composite model-helicopter rotor blades. These items employ a symmetrical airfoil section of chord 55 mm and approximately 14% maximum thickness. The outer tip is strongly raked to provide a smooth termination that is effectively square. As supplied, the inner region is tapered for attachment to a hub. This part was cut off square to provide a constant-chord, 536 mm-span blade for the VAWT model. Four of these were available, allowing two-, three- and four-bladed configurations to be built. On the basis of chord, the scale is approximately one-third of a full-size machine [9].

The blades were positioned on a circle of radius 265 mm, and connected to a central shaft via cylindrical spokes. The shaft and spokes were made as thin as strength and stiffness requirements would allow, having respective diameters 25 and 6 mm. For comparison purposes, a 55 mm-diameter tube could be fitted over the standard shaft to produce a wide-shaft configuration.

Forced-transition configurations were created by attaching zig-zag tape along the blade spans at the maximum thickness point. This modification was made either to the blade inner surfaces, or outer surfaces, or both simultaneously.

B. Test Facility

The VAWT model was tested in a closed-section wind tunnel with a cross-section of 1.68 m width and 1.22 m height. The model was mounted centrally, with its shaft horizontal, as shown in Fig. 3. Sound measurements were taken using

the ‘low-frequency’ 48-microphone flush-mounted array described in Ref. [16]. For the cross-spectra discussed here, a microphone pair almost directly below the shaft axis and with cross-flow separation 118 mm was employed (cf. Fig. 3).

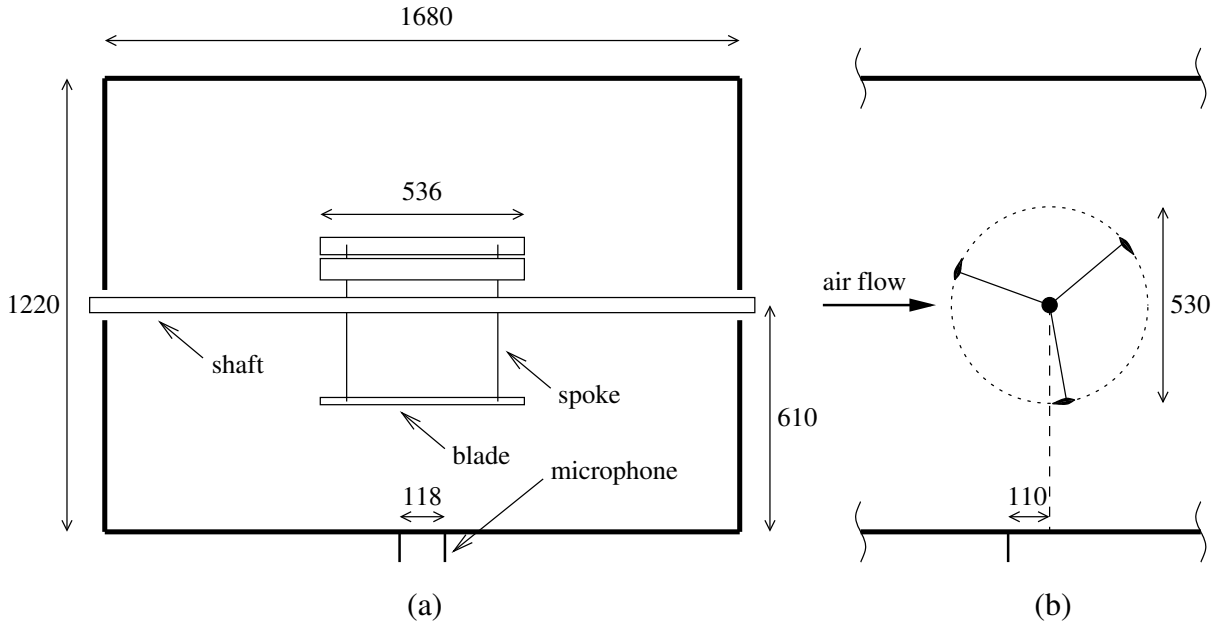

Fig. 3 The model VAWT in the wind tunnel: (a) streamwise view; (b) cross-stream view. Dimensions in mm.

Differing results may be expected depending on whether the blades nearer the microphones travel upstream (‘contra-flow’) or downstream (‘co-flow’). Hence both conditions were tested. Figure 3(b) shows the co-flow arrangement, for which the rotation in this view is anti-clockwise.

The wind-tunnel flow has typical empty-section turbulence intensity 0.15% [17]. To explore the impact of inflow turbulence, unsteadiness levels were artificially raised by placing a turbulence grid upstream of the working section. The grid consists of square 19 mm bars arranged in a mesh with spacing 102 mm. For a tunnel speed of 4.8 m/s, hot-wire measurements at the model location showed a turbulence intensity of 8.2% , with (auto-correlation-based) length-scale 43 mm.

C. Data Acquisition and Processing

The microphone signals were sampled synchronously for 1200 model revolutions (approximately 100 s) at a rate of 2048 per revolution. The sampling is from a uniform stream at a higher rate, leading to a slight non-uniformity in measurement spacing. Hence the raw data were first interpolated to regular intervals via a piecewise-cubic representation. Next, the deterministic components were identified on the basis of a revolution-by-revolution average, and subtracted to yield the stochastic remainders.

For a pair of microphone pressures $p_m(t)$ and $p_n(t)$, the cross-correlation function is defined via

$$R_{mn}(t,\tau) = \overline{p_m(t)p_n(t+\tau)}, \tag{1}$$

where the dependence on t must be retained because the signals are not statistically stationary. They are, however, *cyclo-stationary*; for a fixed τ, R_{mn} is periodic in t. This implies that the cross-spectrum,

$$S_{mn}(t,f) = \int_{-\infty}^{\infty} R_{mn}(t,\tau)\mathrm{e}^{-\mathrm{i}2\pi f\tau}\,\mathrm{d}\tau, \tag{2}$$

can be written as a Fourier series:

$$S_{mn}(t,f) = \sum_{r=-\infty}^{\infty} \hat{S}_{mn}(r,f)\mathrm{e}^{\mathrm{i}r2\pi Ft}, \tag{3}$$

where F is the rotation frequency of the model. Furthermore, in the absence of blade-to-blade variations, many of the Fourier components in Eq. (3) will be zero, as the signals are then cyclo-stationary with the blade-passing frequency.

Clearly cyclo-stationarity complicates the task of signal analysis. However, it can be shown (cf. Appendix A) that a conventional periodogram calculation [18] still yields useful information. Specifically, with block size corresponding to the revolution time, it returns the average over t of the cyclo-stationary cross-spectrum, i.e. $\hat{S}_{mn}(0,f)$. For brevity, this quantity will henceforth be referred to as 'the' cross-spectrum. To form it, the 2048-point data blocks were Hann-windowed before Fourier transformation, and were overlapped at 50%. This yielded 2399 periodograms for averaging, comfortably sufficient to ensure convergence [10]. Finally, the cross-spectrum magnitudes were corrected for the (manufacturer-supplied) microphone frequency responses.

D. Experimental Program

Aeroacoustic noise sources typically exhibit a strong dependence on flow speed, and airfoil self-noise is no exception [14]. To examine the separate effect of TSR variations, it is therefore necessary to fix the relative velocity between flow and blade. In practice, this ideal is unattainable, because the azimuthal variation shown in Fig. 1 is TSR-dependent. As a compromise, the relative velocity at maximum (nominal) incidence, U_r, was held constant. This implies a wind-tunnel speed, U_∞, of $U_r/\sqrt{1+\lambda^2}$, and a blade speed, U_b, of $\lambda U_r/\sqrt{1+\lambda^2}$. The value of U_r was set by the (vibration-related) rotor speed limit, at 21 m/s (comparable to full-scale operation in winds around 6 m/s). The associated tunnel and blade speeds are given in Table 1. All three blade-number configurations were tested under these conditions.

Speed dependence itself was assessed by fixing TSR and varying tunnel velocity. The available range was limited at the low end by tunnel controllability, and at the high end by rotor speed. The latter constraint was relaxed as far as possible by employing the three-bladed rotor (least susceptible to vibration) operating at TSR 3. This allowed tests to be conducted at tunnel velocities between 4 and 8 m/s.

Table 1 Wind-tunnel and blade speeds for a fixed relative velocity of 21 m/s at maximum nominal incidence.

TSR, λ	U_∞ (m/s)	U_b (m/s)
3	6.6	19.9
4	5.1	20.4
5	4.1	20.6

The three-bladed rotor, as a representative configuration, was also used for the runs with boundary-layer trips. These were carried out at the constant-relative-velocity settings of Table 1. The same conditions were employed for wide-shaft testing, but here the two- and four-bladed rotors were chosen, in order to span the full range of induction factor.

Finally, matching empty-tunnel measurements were made to establish background-noise levels. These experiments were carried out with the VAWT-model drive unit running at the speed appropriate to the comparison case.

IV. Results

A. Cross-Spectrum Characteristics

Figure 4 shows a typical cross-spectrum, for the three-bladed model in contra-flow rotation at TSR 4. Also plotted is the background cross-spectrum for this condition. As the frequency scale is logarithmic, the magnitudes have been pre-multiplied by frequency, so that the relative importance of different frequency ranges can be seen directly.

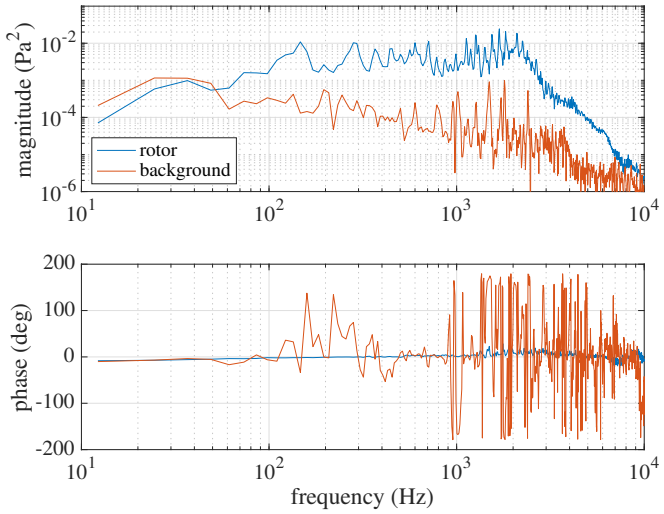

Fig. 4 Frequency-multiplied cross-spectra, $f\hat{S}_{mn}(0,f)$, with ('rotor') and without ('background') turbine model. Three-bladed model in contra-flow configuration, at TSR 4.

The test data are comfortably above the background for frequencies from 70 to 7000 Hz. In this range, the phase is essentially zero, in contrast to that of the background measurement. Departures from zero are generally associated either with a trough in the magnitude, or with a background peak approaching the level of the data. These features are

typical of all the configurations reported here. Their general representativeness has been confirmed via spot checks on other possible choices of microphone pair. (The only differences observed were slightly reduced levels at the higher frequencies for greater separations, indicating coherence loss in the acoustic signal. This undesirable phenomenon is least evident in the cross-spectra presented here.)

Figure 4 provides the justification for assessing the model-scale VAWT's noise on the basis of a single cross-spectrum. The results show that a correlated signal with stable phase has been extracted, and that this signal is not associated with tunnel flow noise. This point would hold even if the phase difference were non-zero. (For example, a sound wave propagating parallel to the tunnel floor and along the line connecting the microphones would give rise to 180 deg phase separation at around 1.5 kHz.) Hence the generally near-zero phase data imply a further conclusion: that the sound comes from a direction closely perpendicular to the microphone-pair axis. This is consistent with its source being the rotor.

Over the reliable data range, significant contributions are evident from about 100 Hz to 3 kHz. At full scale, the corresponding frequencies would be lower. The QR5 turbine has blade chord 175 mm and operates at TSR 3.5 [9]. A simple chord-based Strouhal scaling then gives 30–940 Hz at 6 m/s wind speed, and 50–1570 Hz at 10 m/s. The lower limits are close to the edge of the audible range, where the ear's sensitivity is low. Hence test data below 100 Hz can safely be ignored. Around 1 kHz, however, human hearing is good, and for this reason test data above 3 kHz might be relevant. Thus subsequent spectra will be plotted from 100 Hz to 5 kHz.

Within this frequency range, a notable feature of the cross-spectrum magnitude is its peakiness. (Recall that deterministic harmonics of the rotor frequency have been removed.) One possible cause is the laminar-instability self-noise mechanism, which produces 'quasi-tones' [14]. On the basis of the data presented in Ref. [14], and a simple Strouhal scaling argument, these would be expected between about 1 and 3 kHz. Lower-frequency peaks might be due to vortex shedding from the cylindrical spokes and shaft. (This phenomenon occurs stably at a Strouhal number around 0.2 for the Reynolds numbers applicable here [19]. Corresponding frequencies would be around 40 Hz for the 25.4 mm shaft in a free-stream of 5.1 m/s, and 680 Hz for a 6 mm spoke at a maximum-radius azimuthal velocity of 20.4 m/s.) Finally, the hard-wall wind tunnel is a reverberant environment, so duct resonances are likely to be in evidence.

Returning to the rotor blades, consideration must be given to other possible sources of self-noise: turbulent-boundary-layer trailing-edge noise, separation noise, tip-vortex noise, and trailing-edge-bluntness noise [14]. All are expected to make a smoothly peaked, broadband, contribution. For the first two, the data of Ref. [14] suggest a maximum anywhere between 2 kHz (at zero blade incidence) and 400 Hz (for the nominal incidence at this TSR, 14 deg). For tip-vortex noise, the relevant length-scale depends on tip shape and a corrected incidence angle. A plausible upper limit is about 10% of blade chord, for which the peak Strouhal number of 0.5 [14] gives here a frequency of 2 kHz. Finally, the trailing edge thickness controls the bluntness-noise scaling, and suggests an expected peak value of 4.2 kHz or higher.

Among the potential broadband self-noise components, only trailing-edge/separation noise is expected to contribute

significantly at sub-1 kHz frequencies, and even that should start to roll off below 400 Hz. This feature would be accentuated by the frequency pre-multiplication employed in Fig. 4. The plot, however, is essentially flat from 100 Hz to 1 kHz. One possible explanation is that trailing-edge noise spectra need not necessarily drop off at lower frequencies (c.f. [20, 21], in whose data there is no sign of a broad peak around the appropriate frequency). Alternatively, these components could arise from the other possible contributor identified in Sec. II.C: interaction noise generated by blades in the downstream arc. Support for this explanation is provided by Ottermo et al. [8], whose full-scale beamforming measurements show strong low-frequency radiation from blades passing through that region. Finally, the previous suggestion that the cylindrical spokes could produce tonal noise may well be too simplistic. The spoke speed varies continuously with radius from (near-)zero to the blade speed, and the relative fluid velocity also typically has a component along the spoke axis. Both these characteristics would militate against the coherent vortex shedding necessary for well-defined tonal noise, but one would still expect sound to be radiated.

B. Diagnostic Tests

Here the results of configuration variations specifically designed to answer questions arising from Sec. IV.A are presented. In particular, the influence of wind-tunnel modes is investigated via speed variations (Sec. IV.B.1), the contribution from laminar-boundary-layer instability noise is probed using surface trips (Sec. IV.B.2), and the effect of a wider shaft is considered (Sec. IV.B.3).

1. Wind-Tunnel Speed Variation

At the low Mach numbers employed here, duct-resonance frequencies in the tunnel should be effectively independent of the flow speed. Tonal noise from the rotor, on the other hand, should exhibit a Strouhal frequency scaling (for a given aerodynamic configuration, i.e. TSR).

Figure 5 shows the cross-spectra from the three-bladed model in contra-flow rotation at TSR 3, for tunnel speeds from 4 to 8 m/s. (Note that magnitudes have been successively multiplied by 10 to separate each case.) The pattern of spectral peaks is clearly unchanged below 2 kHz, and even above this many features at fixed frequencies are evident. Dashed lines on the figure indicate specific examples. On this basis, the spectral peaks correspond to duct resonances rather than tonal noise from the rotor.

2. Boundary-Layer Tripping

Laminar-instability noise can be eliminated by forcing transition in the relevant boundary layer. This may lie on either the pressure or the suction surface [22]. The situation is further complicated for a VAWT blade, as the pressure and suction surfaces alternate between outside and inside as the rotor circle is traversed. Thus tests were carried out with each surface tripped individually, and with both tripped.

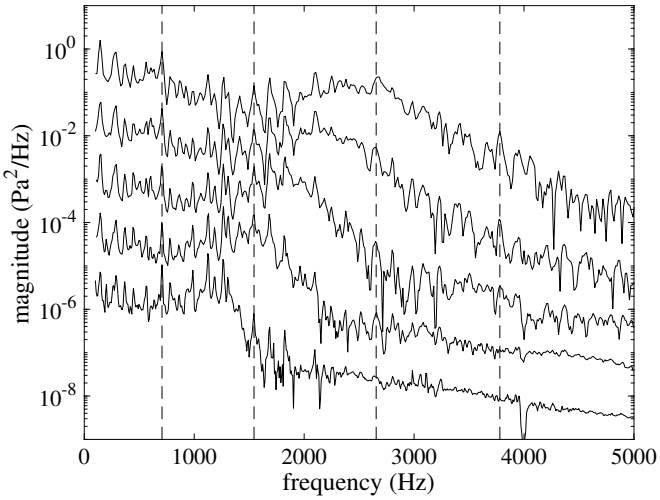

Fig. 5 Offset-magnitude cross-spectra from three-bladed model running at TSR 3 in wind speeds of 4 m/s (bottom), 5 m/s, 6 m/s, 7 m/s and 8 m/s (top).

Figure 6 shows the results for contra-flow rotation at TSR 4. Clear differences between the clean and tripped cases are evident, showing that laminar-instability noise is a significant contributor in the former. Also plotted is the background cross-spectrum for this condition. Despite the reductions associated with tripping, the rotor measurements remain above the background level.

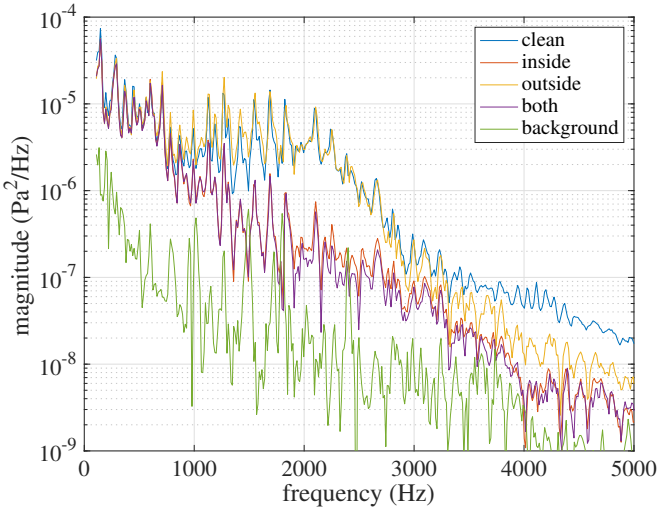

Fig. 6 The effect of boundary-layer trips on the cross-spectrum for the three-bladed model in contra-flow rotation at TSR 4.

Other, subtler, differences present in Fig. 6 will be assessed subsequently in third-octave format. The narrow-band presentation does, however, provide further confirmation that sharp spectral peaks correspond to duct resonances, as these features persist even when both surfaces are tripped. One might then query the apparent absence of the

laminar-instability tones that would be expected in the clean-blade data. A possible explanation is that the instabilities lock on to the duct resonances. This would be plausible behavior, given the nature of the underlying generation mechanism [22–25] and the presence of multiple duct modes in the relevant frequency range.

Turning to the third-octave analysis, Fig. 7 shows the results for all the test configurations. In each case, the inside-surface treatment has the most significant impact, and tripping the outer surface in addition has essentially no further effect. Given this, the inside surface can reliably be identified as the source of the instability. It is then perhaps surprising to see differences arising between the outer-surface-only treatment and the clean blade; both increases (e.g. from 64.9 dB to 69.5 dB for the TSR 5, contra-flow configuration in the 2 kHz band) and decreases (e.g. from 53.6 dB to 48.6 dB in TSR 3 contra-flow at 4 kHz). However, the possibility of coupling between the underlying laminar instability on one airfoil surface and the boundary layer on the other is now well established (cf., for example, [22–24]); while the conditions allowing the instability to develop are local, those governing its final level are not. Hence modification of such coupling by the outer-surface trip seems the most likely explanation for the apparent anomaly.

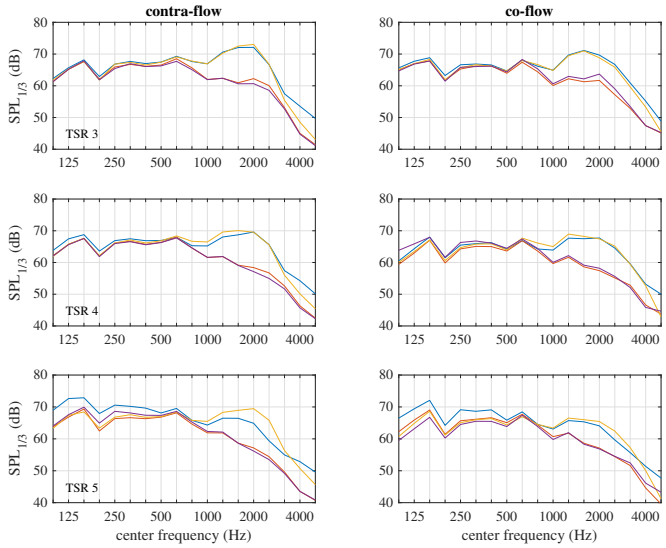

Fig. 7 The effect of boundary-layer trips: third-octave cross-spectrum powers for all configurations. Legend as Fig. 6.

The other obvious question is why laminar-instability noise should be triggered only by the inside surface. A definitive answer is not available; however, the reason must be linked to the differences in the flow experienced by the blades in the upstream and downstream arcs. Both of the features noted previously — asymmetry and wake interactions — are likely to affect the laminar-instability phenomenon. In particular, it is typically only observed in certain incidence ranges.

At lower frequencies, say below 500 Hz, laminar-instability noise is not to be expected in this experiment. The trips might then influence self-noise either by changing boundary-layer properties at the trailing edge or by altering the blade

stall characteristics. Neither possibility seems consistent with the observations; noise reduction is an unlikely outcome for the turbulent-boundary-layer trailing-edge noise mechanism, and a change in stall characteristics would be most evident at the lowest TSR. The low-frequency benefit of tripping at TSR 5 thus remains unexplained. However, it does show that blade sources remain significant even at the lowest frequencies considered here.

3. Shaft size

Wide-shaft tests were carried out for the two- and four-bladed configurations in co-flow rotation. In most cases, the differences from the standard-shaft cross-spectra are negligible; on a narrow-band plot they are hard to distinguish, and discrepancies in third-octave levels are only occasionally as high as 2 dB. The sole exception occurs at 198 Hz for the four-bladed model with TSR 3. Here, as shown in Fig. 8, the wide-shaft value is almost 4 dB below the reference case.

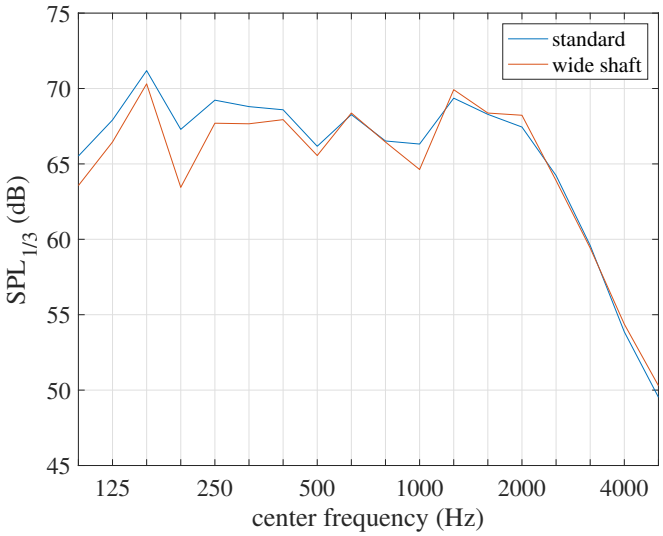

Fig. 8 Effect of increasing shaft width on the third-octave powers for the four-bladed model at TSR 3.

Although 198 Hz is at the low end of the frequencies considered here, it is still well above the vortex-shedding frequency for the wide shaft. Furthermore, a decrease in noise is an unexpected result; on an intuitive basis, the wide shaft should increase any interaction noise from the blades in the downstream arc. A possible counter-argument is that the increased blockage would lead to accelerated flow either side of the shaft, which might mitigate the interaction noise associated with upstream-blade-induced unsteadiness. In this case, however, the effect should be evident at all TSR values. Hence these tests suggest that the shaft has little influence, direct or indirect, on VAWT noise.

C. Parameter Variations

Here the effects of changing operational or configurational parameters are considered. The operational variations are in TSR at fixed relative speed (Sec. IV.C.1) and in speed at fixed TSR (Sec. IV.C.3). The configurational parameter is blade number, whose influence is investigated in Sec. IV.C.2.

1. Effect of TSR

Figure 9 compares the third-octave levels at TSRs 3, 4 and 5, for each of the test configurations. The first point to note is that the dominant trends are consistent between the two rotation directions.

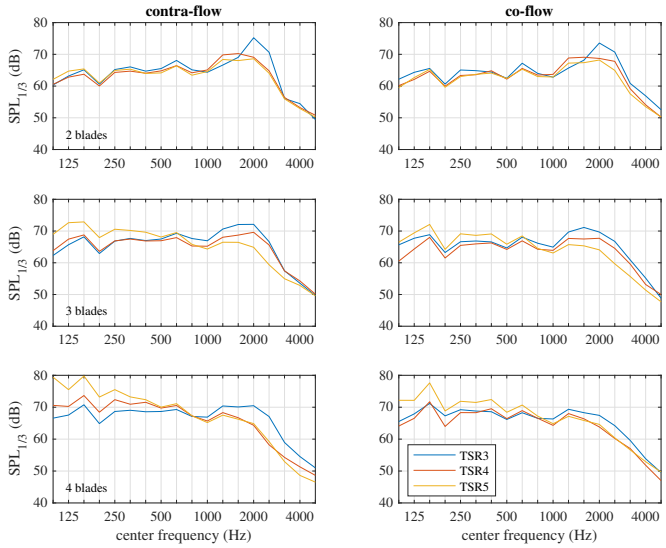

Fig. 9 The effect of tip-speed ratio at a fixed relative velocity of 21 m/s.

The clearest effect is a reduction in higher-frequency noise as TSR increases. On the other hand, for some cases, levels in the sub-500 Hz range rise. This tendency becomes more evident with greater blade number; it is absent for two blades, visible between TSRs 4 and 5 for 3 blades, and arguably present across all three TSRs for 4 blades. (Here there is some discrepancy between rotation directions. Note, however, that the co-flow, TSR-3, 198 Hz point has already been identified as anomalously high in relation to the wide-shaft data.) Thus the overall impact of a TSR increase is only unambiguously beneficial for the two-bladed case, and between TSRs 3 and 4 for the three-bladed case. This point is confirmed by inspection of the summed totals of the third-octave components, which are presented in Tables 2 and 3. For both three- and four-bladed configurations, there is an increase between TSR 4 and TSR 5.

Table 2 Overall SPL for the contra-flow spectra of Fig. 9.

Blades	TSR		
	3	4	5
2	79.6	77.8	77.3
3	80.2	78.9	80.7
4	80.5	81.5	85.5

Close examination of Fig. 9 suggests that increasing blade number has similar effects to increasing TSR. This would imply that the sound-level changes are linked to changes in induction. A complicating factor, however, is the interplay

Table 3 Overall SPL for the co-flow spectra of Fig. 9.

Blades	TSR		
	3	4	5
2	78.8	77.3	76.5
3	79.4	77.6	79.2
4	79.8	79.1	82.7

between noise-per-blade and overall noise. The following section explores this point further.

2. Effect of Blade Number

Broadly speaking, Fig. 9 suggests a tendency for noise levels to increase with blade number at lower frequencies, and to decrease at higher. This point can be assessed more carefully by direct comparisons of the 2-, 3- and 4-bladed configurations at each TSR (Fig. 10). To elucidate how much of the effect is due to aeroacoustic source changes, the results are scaled to give a noise-per-blade comparison; i.e. the 2-bladed levels are multiplied by 3/2 (+1.8 dB) and the 4-bladed levels by 3/4 (-1.2 dB).

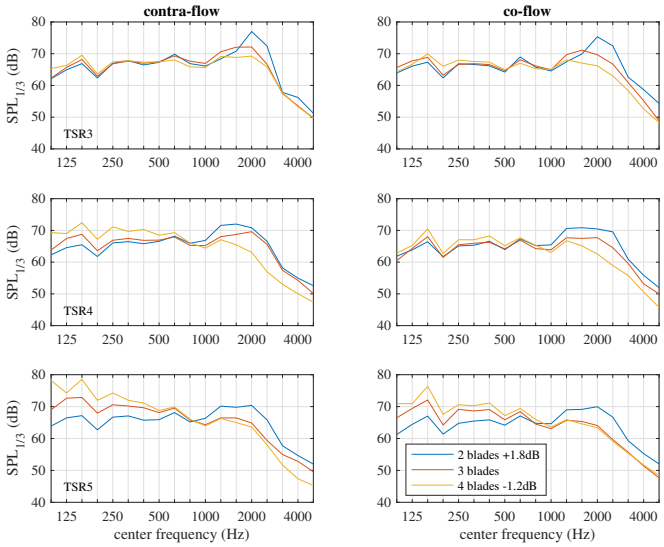

Fig. 10 The effect of blade number at a fixed relative velocity of 21 m/s. Note the adjustment in levels to provide a per-blade comparison.

The plots confirm the broad characterization, with a cross-over between 'low' and 'high' frequencies around 800 Hz. The low-frequency increases with blade number are most marked for the higher TSRs; at TSR 3, the changes seen in Fig. 9 are essentially attributable simply to the presence of more sources. By TSR 5, however, it is clear that the source characteristics too have changed.

For the high-frequency dependence, there is no obvious way in which TSR consistently alters the reduction with

blade number. Here, however, the per-blade behavior counteracts the source-number effect. Hence at TSR 5 in co-flow rotation, the insignificant reduction in per-blade noise in going from 3 to 4 blades corresponds to a slight *increase* in overall level (Fig. 9), whereas the clear drop from 2 to 3 is enough to overcome the associated rise in contributors.

Thus it seems that the dependencies on TSR and blade number can be explained in terms of a single aerodynamic characteristic: induction factor. Large induction factors (associated with higher TSR and more blades) are associated with greater low-frequency source noise levels, and reductions at higher frequencies. The latter are offset, but usually only partially, by the increase in source number when blades are added.

The low-frequency impact suggests a significant rôle for interaction noise in this region. Neither of the other potential contributors — 'atypical' self-noise and spoke noise — would be expected to show this dependence. Even granted errors in the fits of Ref. [14] at low frequencies, the tendency for self-noise to shift to higher frequencies with decreasing incidence (higher TSR) is likely to be robust, and the opposite is observed in Fig. 9. Meanwhile, a much greater increase in rotation speed than here (3.4% from TSR 3 to TSR 5) would be required for the rise to be due to spoke noise. Higher interaction noise is, however, plausible, because induction effects are not steady in the downstream arc. The average reduction in flow velocity there arises from the fluctuations caused by upstream blade passages; hence the larger the induction factor, the larger the fluctuations too. The ensemble average effect of the fluctuations contributes to the periodic noise component not considered here. However, the stochastic part will increase likewise, resulting in more interaction noise.

3. Dependence on Speed

The contra-flow cross-spectra for speed variation at fixed TSR have already been presented in Fig. 5. Clearly evident is a shift towards higher frequencies at higher speeds, consistent with the Strouhal scaling typical of flow-noise problems. That scaling, and the dependence of magnitude on speed, are investigated in this section.

For comparability with previous work, the velocity-scale should be representative of the relative flow speed, which varies between $U_\infty(\lambda - 1)$ and $U_\infty(\lambda + 1)$. Here, the value at maximum blade incidence, denoted U_r, is chosen. The most straightforward length-scale is the blade chord, and the left-hand plot of Fig. 11 shows how the cross-spectra of Fig. 5 collapse when plotted against the associated Strouhal number. The spectrum shapes now align convincingly.

Alternatively, a Strouhal number based on a representative boundary-layer thickness could be used [14]. In particular, given the strong evidence for a significant laminar-instability-noise component, the overall (laminar) boundary-layer thickness δ is indicated [14]. Again, matters are complicated by the changes in blade incidence with rotation. However the expressions suggested in Ref. [14] consist of a speed-independent incidence factor multiplying a zero-incidence thickness given by

$$\delta = c10^{\left[1.6569 - 0.9045 \log_{10} R_c + 0.0596 (\log_{10} R_c)^2\right]}, \tag{4}$$

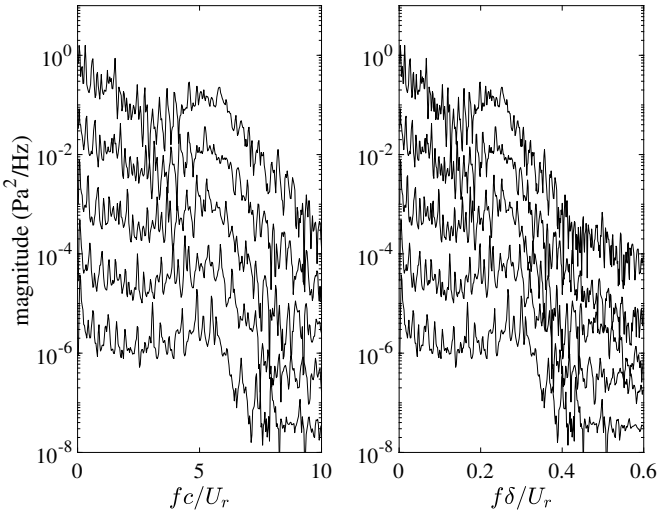

Fig. 11 Offset-magnitude cross-spectra for three-bladed model in contra-flow rotation at TSR 3, plotted against chord-based (left) and boundary-layer-thickness-based (right) Strouhal number. Wind speeds as Fig. 5.

where R_c is the chord-based Reynolds number. Thus, whatever blade position (or combination thereof) is taken as representative, the speed dependence will follow that of Eq. (4). The results obtained by employing this formula are shown in the right-hand plot of Fig. 11. The underlying legitimacy of a Strouhal scaling is again evident via comparison with Fig. 5, and the maxima are found around the expected values of Strouhal number [14]. However, the detail collapse differs from that in the left-hand plot, and it is, if anything, less successful.

The results of the same analyses applied to the co-flow data are shown in Fig. 12. Here differences between the two plots are harder to discern, but there is certainly no clear benefit in choosing the boundary-layer thickness as the length-scale. It should also be noted that the formula for δ has a weaker speed dependence than expected for a laminar boundary layer. This follows from the dimensionless governing equations [26] as $\delta \sim cR_c^{-1/2}$, and a scaling based on this form is unambiguously worse. Hence boundary-layer thickness does not appear to be the relevant length-scale here.

Having established the frequency scaling, the effect of speed on level can be considered. According to the established self-noise theories, overall sound power scales with either U_r^5 (large-chord trailing-edge noise) or U_r^6 (dipole noise). In conjunction with the chord-based Strouhal scaling, this implies a dependence of U_r^4 or U_r^5 for the cross-spectrum magnitude. Figure 13 shows the collapse for the former. While plausible at first sight, close examination reveals a tendency for lower levels at the higher speeds, suggesting that the true dependence is somewhat weaker. Indeed, integrated spectral levels show sound power proportional to U_r^4 rather than U_r^5.

There are several possible reasons for the discrepancy. First, the reverberant wind-tunnel environment will respond differently at different frequencies. Hence a component at a given Strouhal number may be amplified or attenuated relative to its expected level when the speed changes. Second, the theoretical predictions take the source strength (suitably scaled) to be constant. This assumption may well be violated for the laminar-instability contributions, as the

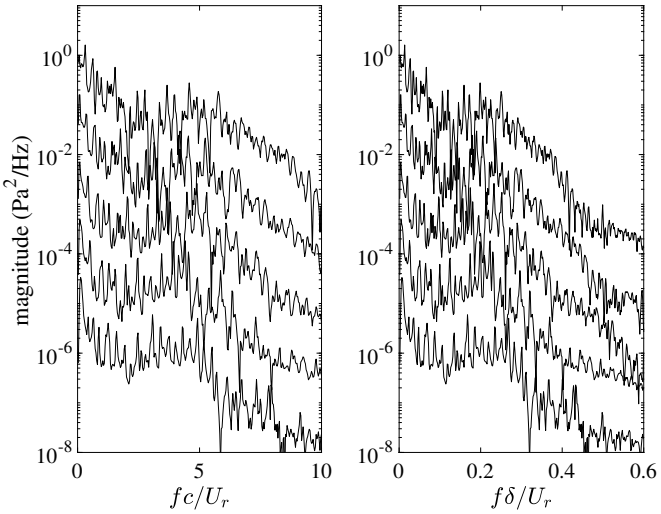

Fig. 12 Offset-magnitude cross-spectra for three-bladed model in co-flow rotation at TSR 3, plotted against chord-based (left) and boundary-layer-thickness-based (right) Strouhal number. Wind speeds as Fig. 5.

level to which they grow is not necessarily set by the overall velocity scale alone. Finally, the far-field approximation employed in the theoretical analyses is likely to be invalid here. (At 1 kHz, the model shaft is under two wavelengths from the microphone pair, and the blades approach as close as one wavelength during rotation.) In the case of the point dipole, the significance of this observation can be seen from the general expression [27], whose near-field contributions have fundamentally different forms than the far-field term.

D. Effect of Inflow Turbulence

Figure 14 compares the measured cross-spectra with and without the turbulence grid in place. Broadly speaking, the impact of the grid is not great. However, a reduction in levels at the higher frequencies is a consistent, and unexpected, feature of the results. Of the noise-generation mechanisms at play, only laminar instability could plausibly exhibit this behavior. There are two ways in which it might come about. One possibility is direct elimination of the instability at these frequencies via turbulence impingement on the blade inner surfaces. The other is interference in the coupled outer-surface response. Which applies remains an open question. However, it is interesting to note the similarity between these results and those in Fig. 7 for outer-surface trips alone.

The only other notable feature of Fig. 14 is a rise in lower-frequency noise at TSR 3. In the light of the foregoing discussion, this is most probably due to interaction between the inflow turbulence and blades in the upstream arc. Such a contribution would decrease with increasing TSR, as the turbulent fluctuations become less significant relative to the blade speed. In conjunction with the previously observed tendency for increases with TSR at these frequencies when the inflow is smooth, this would explain why a similar difference is not obviously evident at TSRs 4 and 5.

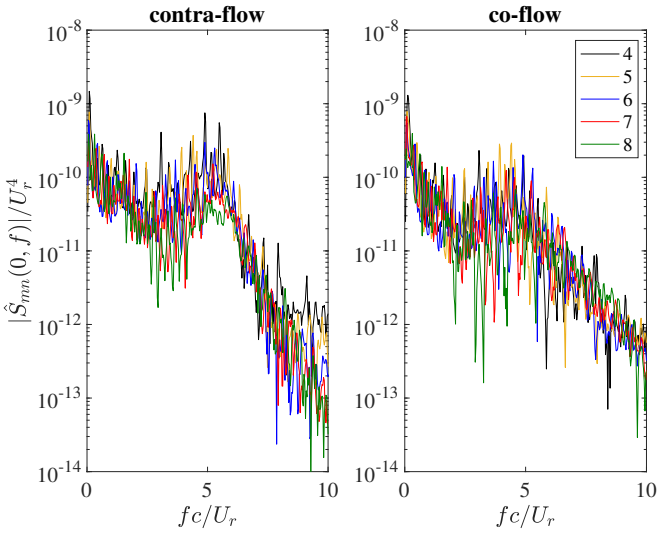

Fig. 13 Scaled cross-spectra for three-bladed model at TSR 3. Legend indicates wind speed in m/s.

E. Summary

The model-scale VAWT has been found to emit significant stochastic noise between about 100 Hz and 3 kHz. At full scale, the corresponding components would have lower frequencies, but would still lie in the audible range.

When the inflow is clean, there is clear evidence of laminar-instability noise associated with the blade inner surfaces. In contrast, there appear to be no such contributions from the outer surfaces.

Apart from components in the range expected for self-noise [14], the cross-spectra also exhibit significant levels at lower frequencies. On this basis, the empirical model of Ref. [14] may be open to question. Other possible causes are spoke noise and interaction noise. The latter would be consistent with observed dependences on TSR and blade number.

Interaction noise may also arise due to the rotor-shaft wake, but experiments with a wide shaft show no strong evidence of a measurable contribution. The same mechanism underlies turbulence-inflow noise. Introducing grid-generated turbulence leads to a slight increase in lower-frequency levels at TSR 3, but has negligible effect at TSRs 4 and 5.

Finally, the results from tests at TSR 3 and varying tunnel speed confirm the expected Strouhal scaling and strong dependence on flow velocity. In contradiction of Ref. [14], though, a Strouhal number based on blade chord leads to a slightly better collapse than one based on boundary-layer thickness.

V. Practical Implications

A full-scale VAWT operates at different Reynolds numbers from the tests reported here, and in a different flow environment. The turbulence-grid tests show inflow unsteadiness having a weak effect, but extending this conclusion to full scale clearly rests on comparability between atmospheric and experimental fluctuation levels. An approximate exploration of this issue is presented in Appendix B. Although not definitive, it suggests that the experimental fluctuations

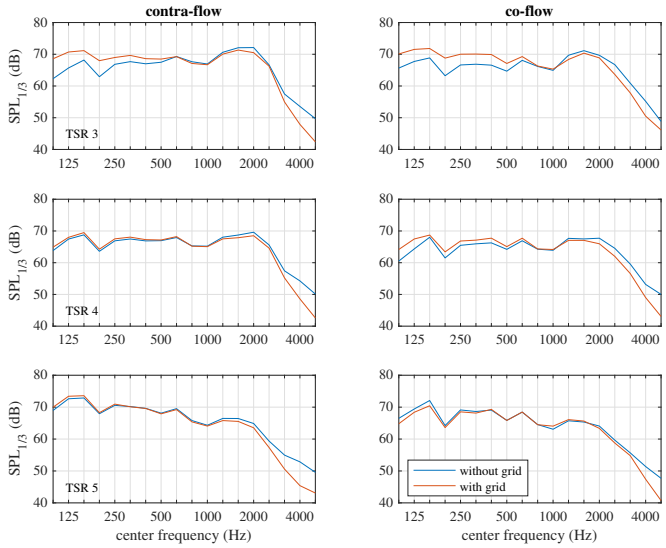

Fig. 14 The effect of inflow turbulence. (Three-bladed model, fixed relative velocity.)

at noise-producing scales comfortably exceed those in atmospheric measurements. If so, inflow-turbulence noise can be discounted.

In the light of recent studies showing inflow-turbulence contributions to low-frequency noise from horizontal-axis machines [28, 29], this suggestion must remain tentative. Note, however, that downstream-arc interaction noise is unique to VAWTs, and this component also occurs at low frequencies. It could thus mask turbulence-inflow noise that would otherwise be evident. In any case, it can reasonably be argued that clean-inflow tests have practical relevance.

Also differing at full scale is the acoustic environment. As has been seen, the reverberant nature of the closed-section wind tunnel is clearly manifested in the microphone cross-spectra. Additionally, the proximity of the microphones to the model makes near-field contributions likely, and the observed speed dependence suggests that they are indeed present. In contrast, the noise nuisance from full-scale VAWTs will almost invariably be experienced in the far field. Nonetheless, the underlying causes of the noise remain the same in both experiment and practice. Only the relative importance and frequency dependence of different components may change. Hence this paper's characterization of VAWT noise, and of its parametric dependence at fixed relative blade speed, should carry over to free-field operation.

Next, consider scale effects. In particular, the laminar-instability noise seen in the experimental results would be expected to disappear at sufficiently large Reynolds number. For the QR5 turbine considered in Ref. [9], with 175 mm-chord blades operating at TSR 3.5 in a wind of 10 m/s, this parameter is approximately 0.4×10^6. Meanwhile, laminar-instability noise is encountered for values up to 1.5×10^6 at least [14]. Hence this phenomenon remains a concern in practice.

In principle, the cure is straightforward, as evidenced by the dramatic cross-spectrum reductions in the experiments with tripped blades. However, there are potential aerodynamic penalties to be considered. Airfoil selection for both low

noise and high performance may thus require careful consideration. In mitigation, this is a problem that should be amenable to simplified testing. Laminar-instability noise during VAWT operation seems highly unlikely for sections that do not suffer from it in a steady, two-dimensional, configuration. Likewise, aerodynamic characteristics in such a configuration will be strongly indicative of performance in reality. On this basis, section optimisation should be possible without excessive development effort.

Finally, one can consider how to specify operational parameters to minimise noise. Here the essential point is that, at aerodynamically viable operating conditions, blade speed matters most. For fixed relative velocity, all the overall contra-flow SPLs bar one lie within 4 dB of one another (Table 2). The same is true of the co-flow values (Table 3). In contrast, the speed-related effect of an increase in TSR from 3 to 5 at fixed wind speed adds 8.3dB to noise levels even if the dependence is only like the fourth power (as observed in these experiments). In reality, as previously argued, far-field noise is more likely to scale with the fifth or sixth power of (relative) velocity, in which case the rise would be 10.4 or 12.4dB. Designs with peak efficiencies at lower TSRs are thus to be preferred. The outliers in Tables 2 and 3 reinforce this conclusion, as they show excess levels at TSR 5.

VI. Conclusions

This paper has reported observations of the stochastic noise from a model-scale VAWT in a wind tunnel, on the basis of cross-spectra from a pair of flush-mounted floor microphones. Significant contributions are present at frequencies from 100 Hz to 3 kHz. The corresponding limits at full scale would typically be 2 to 3 times lower. Other aspects of the measurements are expected to be representative of practical operation (cf. Sec. V).

Noise from sources other than the blades appears to be negligible; there is no strong evidence for significant contributions, either direct or indirect, from spokes and shaft. For the blades, an important generation mechanism is laminar instability, but this is straightforwardly eliminated via boundary-layer tripping. The same should be true in practice, subject to avoidance of possible associated aerodynamic-efficiency penalties. Other blade self-noise mechanisms must be accepted as inevitable.

Interaction noise between the blades and incident flow unsteadiness seems unlikely to be important. However, it can also arise as blades in the downstream rotation arc encounter disturbances from upstream transits, and this is the probable cause of increases in low-frequency (sub-800 Hz) levels for configurations with more blades at higher TSRs.

If the most extreme of these configurations (4 blades, TSR 5) is avoided, and the relative blade speed is held constant, overall noise levels do not vary greatly. Dependence on speed, however, is strong: like the fourth power for the 3-blade, TSR-3 configuration. Even higher exponents are likely for listeners in the acoustic far field. Therefore, to minimise noise at a given wind speed, VAWT designs with peak performance at lower, rather than higher, TSRs should be selected.

Supporting research data are available at: https://doi.org/10.17863/CAM.71406.

Appendix A: Periodogram Analysis Applied to Cyclo-Stationary Signals

The N-point discrete Fourier transform of $p_m(t)$, at frequencies $l\Delta f$, is given by

$$\tilde{p}_m(l\Delta f) = \sum_{j=0}^{N-1} p_m(j\Delta t) \mathrm{e}^{-\mathrm{i}2\pi l\Delta f j\Delta t}, \tag{5}$$

where $\Delta t = 1/f_s$, with f_s the sampling frequency. When this quantity is evaluated using the FFT algorithm, N values at spacing $\Delta f = f_s/N$ are returned. The conventional estimate of the cross-spectrum between p_m and p_n follows from averaging $\widetilde{wp_m}^* \widetilde{wp_n}$, where $w(t)$ is a 'window' function that mitigates spectral leakage by smoothing discontinuities at the edges of the signal blocks.

Applying the same approach here, with the inverse relation

$$R_{mn}(t,\tau) = \int_{-\infty}^{\infty} S_{mn}(t,f) \mathrm{e}^{\mathrm{i}2\pi f\tau} \, \mathrm{d}f \tag{6}$$

used to substitute for the cross-correlation, yields

$$\overline{\widetilde{wp_m}^* \widetilde{wp_n}} = \sum_{j=0}^{N-1} \sum_{k=0}^{N-1} \int_{-\infty}^{\infty} w(j\Delta t) w(k\Delta t) S_{mn}(j\Delta t, f) \mathrm{e}^{-\mathrm{i}2\pi(l\Delta f - f)(k-j)\Delta t} \, \mathrm{d}f. \tag{7}$$

Next, the Fourier-series form of the cross-spectrum, Eq. (3), is introduced, and the summations over j and k carried out. The result is

$$\overline{\widetilde{wp_m}^* \widetilde{wp_n}} = \sum_{r=-\infty}^{\infty} \int_{-\infty}^{\infty} \tilde{w}^*(f - l\Delta f) \tilde{w}(f - l\Delta f - rF) \hat{S}_{mn}(r,f) \, \mathrm{d}f. \tag{8}$$

Like the stationary-signal case, the estimate arises from a convolution of the true spectrum with transforms of the window function. The difference lies in the summation over r and the associated frequency shift of one of the window transforms. With block size corresponding to one rotor revolution (so $\Delta f = F$), the offset is $r\Delta f$.

Now any suitable window function has $\tilde{w}(f)$ concentrated around $f = 0$. Ideally, the focus would be so tight that the only significant contribution to the summation came from $r = 0$, in which case

$$\overline{\widetilde{wp_m}^* \widetilde{wp_n}} = \int_{-\infty}^{\infty} |\tilde{w}(f - l\Delta f)|^2 \, \hat{S}_{mn}(0,f) \, \mathrm{d}f. \tag{9}$$

This is the direct equivalent of the standard result, with the stationary-signal cross-spectrum replaced by $\hat{S}_{mn}(0,f)$.

In practice, $\tilde{w}(f)$ will only reach negligible levels around $f = 2\Delta f$, raising the possibility that Eq. (9) is inaccurate. Against this is the observation (Sec. III.C) that $\hat{S}_{mn}(r,f)$ is only non-zero when r is a multiple of the blade number. The two-bladed configuration is thus most critical. Here, to assess the importance of the contributions from $r = \pm 2$, the microphone signals were re-analyzed with block size corresponding to two revolutions (which sets $\Delta f = F/2$, and

thereby increases the mutual offset between the window functions for $r \neq 0$). Some slight differences were evident in the co-flow cross-spectra; in particular, the double-block-size levels were around 1 dB lower between 4 kHz and 5 kHz. Otherwise the correspondence was very close. On this basis, Eq. (9) is taken to apply; i.e. the experimental results communicated here represent the average over t of $S_{mn}(t, f)$.

Appendix B: Wind-Tunnel versus Atmospheric Turbulence

The grid-generated velocity fluctuations in the inflow-turbulence tests of Sec. IV.D are clearly not directly representative of conditions in full-scale operation. Similarity in velocity spectra thus cannot be expected. Furthermore, even if a field with similar spectra could be manufactured, the components associated with audible noise would still differ. Hence the comparison presented here is necessarily crude, and should be regarded as indicative only.

A straightforward measure applicable to both fields is the turbulence intensity, i.e. the ratio of fluctuation root-mean-square to mean level for the streamwise velocity. Alone, however, this quantity includes contributions from large-scale structures that are irrelevant to noise. Here, then, those contributions are discarded, by estimating the proportion of the streamwise velocity spectrum that they represent. The remainder is used to define an 'effective' turbulence intensity associated with audible noise. This is the turbulence intensity that would be calculated if the fluctuation measurements were first passed through an ideal filter which blocked all sub-audible frequencies.

In the wind-tunnel case, it has been argued that the lowest frequencies relevant to noise at full scale are those in the 100 Hz third-octave band. This has its lower limit at 88.4 Hz. For the nominal relative velocity of 21 m/s, the corresponding turbulence structures have size 0.24 m, and these structures pass the hot wire at speed U_∞. Hence they give rise to fluctuations in the hot-wire signal at frequency $U_\infty/(0.24)$ Hz.

Figure 15 shows the spectrum $S_{uu}(f)$ of streamwise velocity fluctuations at a tunnel speed of 4.8 m/s. Also plotted is the $-5/3$ dependence expected in the inertial subrange of fully-developed isotropic turbulence. In contrast to atmospheric measurements, there is no extended region with this slope, confirming the expectation of dissimilar spectra. The dashed line shows the lowest frequency relevant for audible contributions at this speed: 20 Hz. The proportion of the spectrum energy above this frequency, estimated via numerical integration, is 56%. The overall spectrum energy follows from the turbulence intensity (8.2%) as $(0.082U_\infty)^2$. Hence the energy of the relevant content is $0.0038U_\infty^2$, yielding an effective turbulence intensity of 6.2%.

Information on atmospheric turbulence is available in Refs. [30] and [31]. Here, the velocity spectra for stable atmospheres were shown to collapse to a general form with frequency dependence

$$\frac{1}{\left[1 + 0.16(f/f_r)^{5/3}\right]}, \tag{10}$$

where f_r is a reference frequency dependent on the degree of stability [31]. Its value can be estimated from the

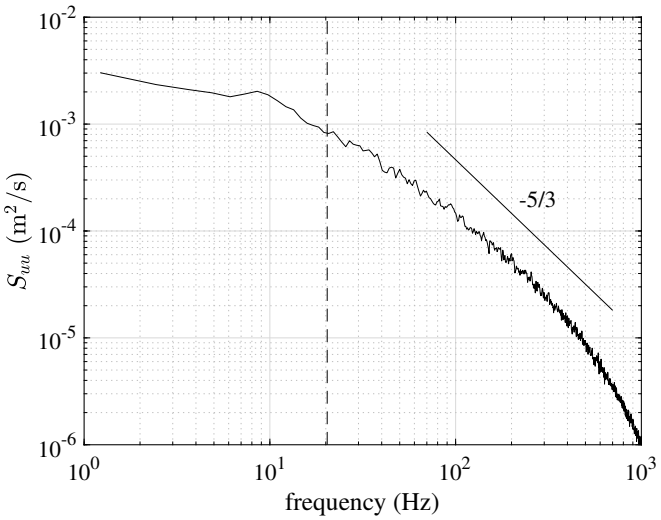

Fig. 15 Spectrum of streamwise velocity fluctuations in grid-generated turbulence.

frequencies given in Ref. [31] for the peak in $fS_{uu}(f)$. In the neutral-stability case, $f_r \approx 0.016U_\infty/h$, where h is the height above the ground. Of the heights where measurements were taken [30], 11.31m is appropriate to a small-wind-turbine installation, and a wind speed of 7 m/s is representative of both the measurements and envisaged operating conditions. These values give 0.0099 Hz for f_r. Meanwhile, the minimum relevant frequency is determined by the limit of audibility (say 20 Hz) and the ratio of noise-generation frequency to measured frequency. For an eddy of a given size, the former is proportional to blade speed, and the latter to wind speed, so the ratio is the TSR (say 4), placing the frequency limit around 5 Hz. The relevant proportion of the fluctuation energy can now be estimated from numerical integration of Eq. 10, at 2.5%.

The overall turbulence intensity is generally below 15% for the neutral-atmosphere data [30]. Therefore the effective turbulence intensity, derived as previously, is below 2.4%. This is notably smaller than the wind-tunnel value.

Consider now how variations in the assumed atmospheric state might affect the calculation. If the atmosphere is unstable the measured spectra are less reliable [31]. However, they roll off at significantly lower frequencies, reducing the proportion of relevant fluctuations. Additionally, the gusty conditions associated with the unstable state are liable to mask the turbine noise. The stable state, however, has spectra with greater high-frequency content, albeit with typically lower wind speeds and turbulence intensities. Neglecting the attenuating effect of the latter factors, and taking f_r to be ten times greater (corresponding to the most stable case documented), increases the effective-turbulence-intensity figure to 5.1%. This is still below the wind-tunnel value.

These results must be qualified by the context of the atmospheric measurements; they were made over flat, open terrain, very different from the urban settings envisaged for VAWTs. Hence they do not unquestionably imply that turbulence-inflow noise is more significant in the wind-tunnel experiment than it would be at full scale. However, they

do provide support for practical relevance as far as the wind-tunnel results are concerned.

Acknowledgments

The second author received a Doctoral Training Grant from the UK Engineering and Physical Sciences Research Council under grant number EP/P505445/1. Support for the experiments was provided by Quiet Revolution Ltd. Tamas Berténi, as Technical Director of Quiet Revolution Ltd., was the prime mover behind this work. The first author is also grateful to Phil Joseph for sharing his expertise on airfoil self-noise, to Peter Davidson for advice on turbulence spectra, and to Simon McIntosh for providing Fig. 2. Finally, the comments of the anonymous reviewers led to significant improvements on the original submission.

References

[1] Banas, J. F., and Sullivan, W. N., "Sandia Vertical-Axis Wind Turbine Program. Technical quarterly report, October–December 1975," Tech. Rep. SAND76–0036, Sandia Labs., Albuquerque, N. Mex.(USA), 1976.

[2] Ffowcs Williams, J. E., and Hawkings, D. L., "Sound generation by turbulence and surfaces in arbitrary motion," *Philosophical Transactions of the Royal Society of London. Series A, Mathematical and Physical Sciences*, Vol. 264, No. 1151, 1969, pp. 321–342. doi:10.1098/rsta.1969.0031.

[3] Mohamed, M., "Aero-acoustics noise evaluation of H-rotor Darrieus wind turbines," *Energy*, Vol. 65, 2014, pp. 596–604. doi:10.1016/j.energy.2013.11.031.

[4] Botha, J., Shahroki, A., and Rice, H., "An implementation of an aeroacoustic prediction model for broadband noise from a vertical axis wind turbine using a CFD informed methodology," *Journal of Sound and Vibration*, Vol. 410, 2017, pp. 389–415. doi:10.1016/j.jsv.2017.08.038.

[5] Ghasemian, M., and Nejat, A., "Aero-acoustics prediction of a vertical axis wind turbine using Large Eddy Simulation and acoustic analogy," *Energy*, Vol. 88, 2015, pp. 711–717. doi:10.1016/j.energy.2015.05.098.

[6] Su, J., Lei, H., Zhou, D., Han, Z., Bao, Y., Zhu, H., and Zhou, L., "Aerodynamic noise assessment for a vertical axis wind turbine using Improved Delayed Detached Eddy Simulation," *Renewable Energy*, Vol. 141, 2019, pp. 559–569. doi:10.1016/j.renene.2019.04.038.

[7] Möllerström, E., Ottermo, F., Hylander, J., and Bernhoff, H., "Noise emission of a 200 kW vertical axis wind turbine," *Energies*, Vol. 9, No. 1, 2016, p. 19. doi:10.3390/en9010019.

[8] Ottermo, F., Möllerström, E., Nordborg, A., Hylander, J., and Bernhoff, H., "Location of aerodynamic noise sources from a 200 kW vertical-axis wind turbine," *Journal of Sound and Vibration*, Vol. 400, 2017, pp. 154–166. doi:10.1016/j.jsv.2017.03.033.

[9] Pearson, C. E., "Vertical axis wind turbine acoustics," Ph.D. thesis, University of Cambridge, 2014. doi:10.17863/CAM.14070.

[10] Pearson, C. E., and Graham, W. R., "Experimental characterization of vertical-axis wind turbine noise," *The Journal of the Acoustical Society of America*, Vol. 137, No. 1, 2015, pp. EL111–EL116. doi:10.1121/1.4904915.

[11] Wilson, R. E., "Wind-turbine aerodynamics," *Journal of Wind Engineering and Industrial Aerodynamics*, Vol. 5, No. 3-4, 1980, pp. 357–372. doi:10.1016/0167-6105(80)90042-2.

[12] McIntosh, S. C., "Wind energy for the built environment," Ph.D. thesis, University of Cambridge, 2009.

[13] Oerlemans, S., "Wind turbine noise: primary noise sources," Tech. Rep. NLR-TP-2011-066, National Aerospace Laboratory NLR, 2011.

[14] Brooks, T. F., Pope, D. S., and Marcolini, M. A., "Airfoil self-noise and prediction," Tech. Rep. NASA-RP-1218, NASA, 1989.

[15] Amiet, R., "Acoustic radiation from an airfoil in a turbulent stream," *Journal of Sound and Vibration*, Vol. 41, No. 4, 1975, pp. 407–420. doi:10.1016/S0022-460X(75)80105-2.

[16] Shin, H.-C., Graham, W. R., Sijtsma, P., Andreou, C., and Faszer, A. C., "Implementation of a phased microphone array in a closed-section wind tunnel," *AIAA Journal*, Vol. 45, No. 12, 2007, pp. 2897–2909. doi:10.2514/1.30378.

[17] Berténgi, T., and Graham, W. R., "Experimental observations of the merger of co-rotating wake vortices," *Journal of Fluid Mechanics*, Vol. 586, 2007, p. 397–422. doi:10.1017/S0022112007006891.

[18] Welch, P., "The use of fast Fourier transform for the estimation of power spectra: a method based on time averaging over short, modified periodograms," *IEEE Transactions on Audio and Electroacoustics*, Vol. 15, No. 2, 1967, pp. 70–73. doi:10.1109/TAU.1967.1161901.

[19] Bearman, P. W., "On vortex shedding from a circular cylinder in the critical Reynolds number régime," *Journal of Fluid Mechanics*, Vol. 37, No. 3, 1969, p. 577–585. doi:10.1017/S0022112069000735.

[20] Moreau, D. J., Brooks, L. A., and Doolan, C. J., "Broadband trailing edge noise from a sharp-edged strut," *The Journal of the Acoustical Society of America*, Vol. 129, No. 5, 2011, pp. 2820–2829. doi:10.1121/1.3569698.

[21] Chong, T. P., Vathylakis, A., Joseph, P. F., and Gruber, M., "Self-noise produced by an airfoil with nonflat plate trailing-edge serrations," *AIAA Journal*, Vol. 51, No. 11, 2013, pp. 2665–2677. doi:10.2514/1.J052344.

[22] Yakhina, G., Roger, M., Moreau, S., Nguyen, L., and Golubev, V., "Experimental and analytical investigation of the tonal trailing-edge noise radiated by low Reynolds number aerofoils," *Acoustics*, Vol. 2, No. 2, 2020, pp. 293–329. doi: 10.3390/acoustics2020018.

[23] Desquesnes, G., Terracol, M., and Sagaut, P., "Numerical investigation of the tone noise mechanism over laminar airfoils," *Journal of Fluid Mechanics*, Vol. 591, 2007, pp. 155–182. doi:10.1017/S0022112007007896.

[24] Arcondoulis, E., Doolan, C. J., Zander, A. C., Brooks, L. A., and Liu, Y., "An investigation of airfoil dual acoustic feedback mechanisms at low-to-moderate Reynolds number," *Journal of Sound and Vibration*, Vol. 460, 2019, p. 114887. doi:10.1016/j.jsv.2019.114887.

[25] Chong, T., Joseph, P., and Kingan, M., "An investigation of airfoil tonal noise at different Reynolds numbers and angles of attack," *Applied Acoustics*, Vol. 74, No. 1, 2013, pp. 38–48. doi:10.1016/j.apacoust.2012.05.016.

[26] White, F. M., *Viscous Fluid Flow*, McGraw-Hill (International Edition), 2006, Chap. 4.

[27] Lowson, M., "The sound field for singularities in motion," *Proceedings of the Royal Society of London. Series A. Mathematical and Physical Sciences*, Vol. 286, No. 1407, 1965, pp. 559–572. doi:10.1098/rspa.1965.0164.

[28] Buck, S., Oerlemans, S., and Palo, S., "Experimental characterization of turbulent inflow noise on a full-scale wind turbine," *Journal of Sound and Vibration*, Vol. 385, 2016, pp. 219–238. doi:10.1016/j.jsv.2016.09.010.

[29] Buck, S., Oerlemans, S., and Palo, S., "Experimental validation of a wind turbine turbulent inflow noise prediction code," *AIAA Journal*, Vol. 56, No. 4, 2018, pp. 1495–1506. doi:10.2514/1.J056134.

[30] Izumi, Y., "Kansas 1968 field program data report," Tech. Rep. AFCRL-72-0041, Air Force Cambridge Research Laboratory, Bedford, MA, 1971.

[31] Kaimal, J. C., Wyngaard, J. C., Izumi, Y., and Coté, O. R., "Spectral characteristics of surface-layer turbulence," *Quarterly Journal of the Royal Meteorological Society*, Vol. 98, No. 417, 1972, pp. 563–589. doi:10.1002/qj.49709841707.